This is the accepted manuscript made available via CHORUS. The article has been published as:

Spin splitting tunable optical band gap in polycrystalline GdN thin films for spin filtering

G. L. S. Vilela, G. M. Stephen, X. Gratens, G. D. Galgano, Yasen Hou, Y. Takamura, D. Heiman, A. B. Henriques, G. Berera, and J. S. Moodera

Phys. Rev. B **109**, L060401 — Published 2 February 2024

DOI: 10.1103/PhysRevB.109.L060401

Spin Splitting Tunable Optical Bandgap in Polycrystalline GdN Thin Films for Spin Filtering

G. L. S. Vilela[1,2], G. M. Stephen[3,4], X. Gratens[5], G. D. Galgano[5,6], Yasen Hou[1], Y. Takamura[7], D. Heiman[1,3], A. B. Henriques[5], G. Berera[8] and J. S. Moodera[1,9]

[1] Plasma Science and Fusion Center, and Francis Bitter Magnet Laboratory, Massachusetts Institute of Technology, Cambridge, MA 02139, USA
[2] Física de Materiais, Escola Politécnica de Pernambuco, UPE, Recife, PE 50720-001, Brazil
[3] Department of Physics, Northeastern University, Boston, MA 02115, USA
[4] Laboratory for Physical Sciences, College Park, MD, 20740, USA
[5] Instituto de Física, Universidade de São Paulo, São Paulo, SP 05508-090, Brazil
[6] Departamento de Física, Universidade Federal de Ouro Preto, Ouro Preto, MG, 35402-136, Brazil
[7] School of Engineering, Tokyo Institute of Technology, 2-12-1 Ookayama, Meguro-ku, Tokyo, 152-8550, Japan
[8] Department of Materials Science and Engineering, Massachusetts Institute of Technology, Cambridge, MA 02139, USA
[9] Department of Physics, Massachusetts Institute of Technology, Cambridge, MA 02139, USA

E-mail: gilvania.vilela@upe.br; Moodera@mit.edu; Heiman@neu.edu

Abstract

Rare-earth nitrides, such as gadolinium nitride (GdN), have great potential for spintronic devices due to their unique magnetic and electronic properties. GdN has a large magnetic moment, low coercitivity and strong spin polarization suitable for spin transistors, magnetic memories and spin-based quantum computing devices**.** Its large spin splitting of the optical bandgap functions as a spin-filter that offers the means for spin-polarized current injection into metals, superconductors, topological insulators, 2D layers and other novel materials. As spintronics devices require thin films, a successful implementation of GdN demands a detailed investigation of the optical and magnetic properties in very thin films. With this objective, we investigate the dependence of the direct and indirect optical bandgaps (E_g) of half-metallic GdN, using the trilayer structure AlN(10 nm)/GdN(*t*)/AlN(10 nm) for GdN film thickness *t* in the ranging from 6 nm to 350 nm, in both paramagnetic (PM) and ferromagnetic (FM) phases. Our results show a bandgap of 1.6 eV in the PM state, while in the FM state the bandgap splits for the majority (0.8 eV) and minority (1.2 eV) spin states. As the GdN film becomes thinner the spin split magnitude increases by 60%, going from 0.290 eV to 0.460 eV. Our results point to methods for engineering GdN films for spintronic devices.

1. Introduction

Spintronic devices based on rare-earth nitrides (RENs) are of great interest since they present both semiconducting and ferromagnetic properties, making these materials suitable for exploiting the spin of carriers in fundamental and applied research [1-2]. Among many RENs, gadolinium nitride (GdN) is especially promising for implementations that aim to explore the electron's spin to store, process and transmit information. The advantageous properties of GdN are its high degree of spin polarization, half-metallic behavior that is useful for spin-filtering, sizeable ferromagnetic transition temperature of ~ 70 K, and large magnetic moment of $7\boldsymbol{\mu_B}/Gd^{3+}$ due to fully occupied 4f electronic states [3-9]. The use of this material in selective transmission of electrons based on their spin orientation finds applications in magnetic tunnel junction, spin valves, spin transistors, and spin-based quantum computing, where the electron's spin state encodes and processes quantum information. In this context, the spin-filtering ability promotes an efficient way to inject and manipulate the spin current [10-15].

Due to its high oxophilicity, GdN easily reacts in air forming Gd_2O_3, which can cause significant changes in its electronic and magnetic properties [16-17]. The growth of stoichiometric GdN thin films, with low levels of oxygen, is very challenging and requires a rigorous control of the synthesis. This challenge has led to some disagreement in the literature regarding the electronic properties of GdN films, but most results point to its semiconducting behavior with an average bandgap of 1.2 to 1.3 eV at room temperature [5, 18-19]. In addition to controlling the stoichiometry, to combine GdN with novel materials that are aimed at investigating interface and spin phenomena, it is crucial to obtain atomically flat surfaces with a high degree of crystallinity, large magneto-optical effects, thermal stability and tunable bandgap energy. These properties depend on the film's strain, thickness, nitrogen vacancies, amount of oxygen impurities, parameters that depend on growth and post-growth processes, as well as protective layers and substrates choices.

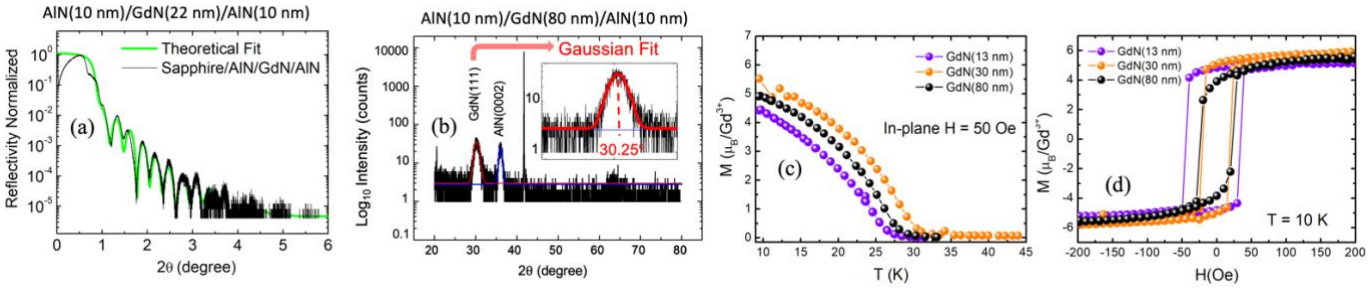


Figure 1. (a) X-ray reflectivity for the RF-sputtered AlN(10 nm)/GdN(22 nm)/AlN(10 nm) and theoretical fit used to obtain the GdN film thickness. (b) High resolution X-ray diffraction pattern for AlN(10 nm)/GdN(350 nm)/AlN(10 nm) on a (0001)- oriented sapphire (Al_2O_3) substrate. (c) In-plane field cooled (FC) magnetization at 50 Oe for GdN thicknesses of 13 nm, 30 nm and 80 nm. (d) Magnetization (M) versus in-plane applied magnetic field (H) at a T=10 K for AlN(10 nm)/GdN(t)/AlN(10 nm) structures, with t = 13, 30 and 80 nm.

In this work, we investigate the optical and magnetic properties of a set of polycrystalline GdN thin films with thickness ranging from t = 6 nm to 350 nm. The AlN(10 nm)/GdN(t)/AlN(10 nm) structures were reactively sputtered on sapphire (0001) substrates in a UHV sputtering system, grown at 700 ℃ in a pressure of 2.8 mTorr (mixture of 40% N_2 and 60% Ar). Measurements using a superconducting quantum interference device (SQUID) magnetometer confirm that the GdN films are magnetic with magnetization saturation of 6 μ_B/Gd^{3+} and a Curie temperature of ~ 30 K, in agreement with previous reports, and X-ray diffraction data confirms a polycrystallinity [5,19-20]. Direct and indirect bandgap energies as a function of the films' thicknesses are determined from analysis of the squared absorption spectra (α^2) and $\sqrt{\alpha}$ using extrapolated curves, respectively. The bandgap energy in the paramagnetic (PM) phase, at 300 K, reveal a direct bandgap of ~ 1.6 eV for the upper spin-split level, whereas this value decreases and splits to 1.2 eV and 0.8 eV, approximately, in the ferromagnetic (FM) phase at 6K. In the low-temperature FM state a well-separated spin-split band energy of $\Delta E = E_\uparrow - E_\downarrow \approx 0.4$ eV is found, which confirms a giant optical spin splitting in the GdN films, where $E_\uparrow$ and $E_\downarrow$ correspond to the bandgaps of the majority and minority states. We also observe the splitting magnitude depends strongly on the GdN film thickness, going from 0.290 eV for a 350 nm thick film to 0.460 eV for a 6 nm thick film, an increase of about 60%.

Since the investigated GdN films are polycrystalline, the extensively used Tauc method suitable for determining the bandgap of amorphous semiconductors wasn't applied in our analysis [21]. Zanatta proposed the use of sigmoid (Boltzmann) functions for more accuracy, and showed that for crystalline Si, Ge and GaAs the α^2 extrapolated curves is in good agreement with the Boltzmann analysis [22]. For simplicity, we used α^2 for direct bandgap estimation.

2. Sample Preparation, Crystal Structure and Magnetic Properties

GdN thin films with thickness ranging from 6.3 nm to 350 nm were deposited on (0001)-oriented sapphire substrates, with buffer and capping layers of 10 nm-thick aluminum nitride (AlN) films to avoid oxidation. The growth process of AlN and GdN took place in a high vacuum sputtering chamber with a base pressure below $\mathbf{5 \times 10^{-8}}$ Torr. To improve the substrate's surface crystallinity and film quality, prior to deposition the sapphire substrates were annealed in a quartz-tube oven at **1100** ℃ for 8 hours in an O_2 atmosphere. After the annealing treatment, the substrates were cleaned in an ultrasonic tank first in acetone, and then in isopropanol before transferring into the load lock chamber and subsequently to the main sputtering chamber. Inside the growth chamber the substrates were slowly heated up to 700 ℃ for degassing followed by the deposition process. Targets of 99.99% purity of Al and Gd were pre-sputtered for 10-20 mins in a controlled atmosphere composed of 60 % Argon and 40 % N_2 before reactively growing AlN and GdN on the substrates. The AlN deposition rate was approximately 1.0 nm/minute, at 700 ℃**,** with an RF power of 150 W and a working pressure of 1.2 mTorr. The GdN films deposition rate was approximately 2 nm/minute were deposited at 700 ℃**,** in a working pressure of 2.8 mTorr and a DC power of 50 W. The deposition rates and film's thickness were estimated using X-ray reflectometry as shown in Fig 1(a). The high-resolution X-ray diffraction (HXRD) patterns for GdN(80 nm) shown in Fig. 1(b) confirm a preferentially orientated growth along the (111) direction in agreement with previous investigations [23-24].

Besides having good crystallinity, it is important that GdN films have a large magnetic moment as confirmed by SQUID measurements, shown in Fig. 1(c) and 1(d). The field-cooled (FC) magnetization curves of GdN film in the trilayer AlN(10 nm)/GdN(t)/AlN(10 nm) show a magnetization saturation varying from 4.5 $\boldsymbol{\mu_B}/Gd^{3+}$ to 5.5 $\boldsymbol{\mu_B}/Gd^{3+}$ for an in-plane $\boldsymbol{H = 200}$ Oe, as the GdN's thickness ranges from t = 13 nm to 80 nm. The FM critical temperature (T_C), was near 30 K, measured with an applied in-plane magnetic field of 50 Oe, as shown in Fig. 1 (d), which agrees with previous reports [5, 19-20]. The coercivity ($\boldsymbol{H_c}$) is larger (40 Oe) for the thinner 13 nm thick GdN film and decreases to ~ 20 Oe for t = 30 and 80 nm.

The observed magnetic moments are smaller than the theoretical expected value of 7 μ_B/Gd^{3+}. One reason is the 200 Oe applied field is not enough to saturate the film, instead it is necessary ~10^4 Oe [12, 25-26]. Other facts might affect the magnetic moment in GdN films: (i) nitrogen vacancies cause changes in the lattice constant, magnetization and conductivity, since N acts as a dopant; (ii) oxygen contamination that also act as dopant; and (iii) lattice parameter strains caused by mismatch between substrate and film [1, 8, 23, 27]. Khazen et al. showed an extension of 2.4 % in the lattice parameter of GdN films, compared to the bulk value of 4.99 Å, promotes substantial changes in the magnetization behavior and reduces the magnetic moment [26]. As shown in the inset of Fig. 1(b), the GdN(111) peak for the 80 nm-thick film is located at $2\theta = 30.25°$ determined by a Gaussian fit. This corresponds to a lattice parameter of 5.11 Å, an extension of 2.4 %. The same analysis for the 350 nm thick GdN presented a (111) peak located at $2\theta = 30.51°$ with a lattice parameter of 5.07 Å, which corresponds to an extension of 1.6 %. The full width at half maximum (FWHM) of the XRD (111) peak for GdN(80 nm) was 1.42° and the crystallite size estimation was 5.8 nm. For GdN(350 nm) these values became 1.01° and 7.8 nm, respectively. The FWHM increase indicates a relaxation of the tensile stress and a reduction in the number of grains due to their coalescence leading to more a crystalline film as GdN becomes thicker.

Finally, the twinned domains present in GdN grains, influenced by the hexagonal surface symmetry of the AlN template/buffer layer, could potentially impact the magnetic and optical properties. This is attributed to the alterations in structural and surface properties observed in group-III rare earth nitrides [28-29].

3. Optical Bandgap Properties

Engineering the optical bandgap in GdN thin films by controlling its magnetic state and thickness leads the way for its implementation in spintronic devices. The temperature dependence of semiconductor's bandgap can be different in bulk and thin film morphologies due to factors such as quantum confinement and lattice strain effects. In bulk samples, the bandgap typically increases as the temperature decreases partly due to the renormalization of electron-phonon interactions and partly due to lattice thermal expansions. As the temperature decreases, the phonon population also decreases leading to an increase of the bandgap energy, making it more difficult for electrons to be excited to the conduction band [30]. In most bulk semiconductors, the thermal expansion term is negligible in first approximation compared to the electron–phonon interaction [30]. In contrast, the bandgap's temperature dependence in thin films is more complex. It is known that light absorption by electrons in semiconductors with restricted geometry like thin films, nanowires, and quantum dots are strongly dependent on the size [32-33]. This quantum confinement effect also gives rise to changes in the transition probabilities, which is a consequence of the electron's wave properties. Materials with

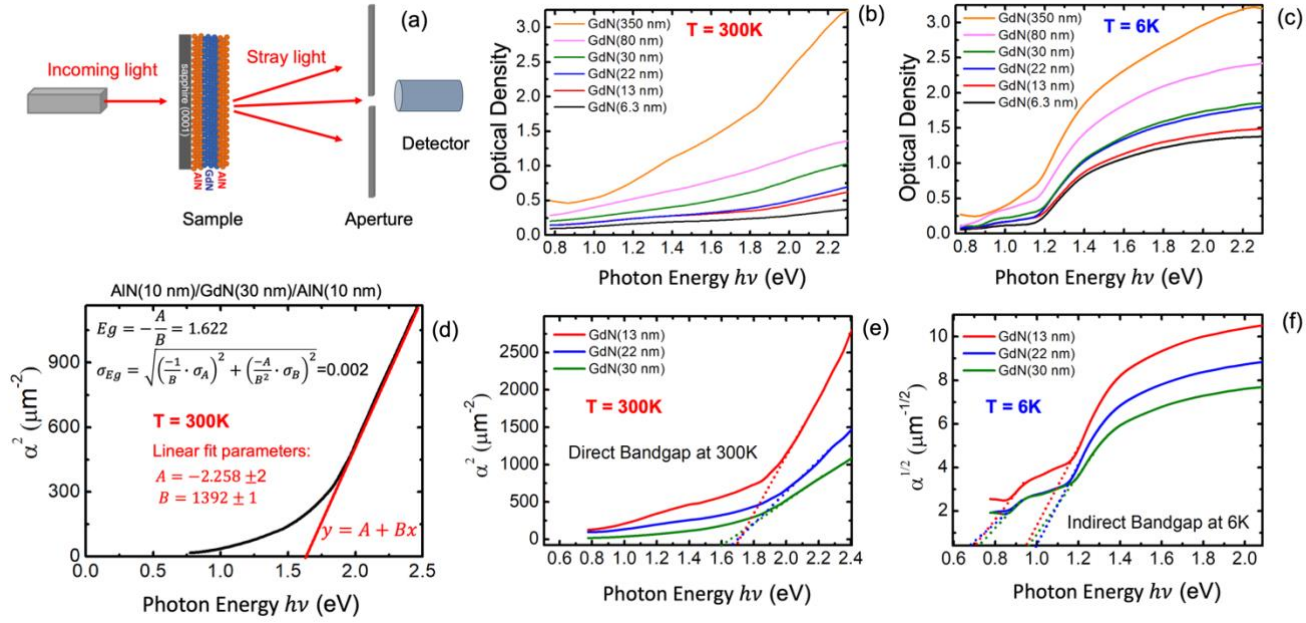


Figure 2. (a) Illustration of the optical density acquisition apparatus composed of light source, sample, aperture, and light detector. (b) and (c) show the optical density (OD) spectra for the set of samples at 300 K and at 6 K. (d) shows how the direct optical bandgap, at room T, for a t = 30 nm thick film was extracted from the squared-absorption coefficient (α) versus photon energy. The linear red fitted curve ($y = Ax + B$) is used to determine the bandgap. (e) and (f) show α^2 and $\alpha^{1/2}$ versus the photon energy $E = h\nu$ for determining the direct and indirect optical bandgaps of the GdN thin films, respectively. The dashed lines indicate the linear extrapolation to $y = 0$ where the intersection corresponds to the direct/indirect bandgap energy.

dimensions on the order of the de Broglie wavelength show relevant quantum-mechanical effects with size-dependent optical properties. Models predict a decrease in phonon frequency and dielectric constant of semiconducting nanostructures leading to an increase of the bandgap energy as the material's size reduces, as confirmed by reported studies [34-36].

On the other hand, the lattice constant plays an important role in the optical, electronic, and magnetic properties of GdN thin films leading to changes on its spin dependent band structure. Previous investigations showed how changes in the unit cell volume of GdN leads to half-metallic to semiconducting transformation [7]. At low temperatures, the lattice constant of the material shrinks, resulting in an increased interatomic bond strength, higher phonon frequencies and reduced lattice vibrational amplitudes [37]. Also, the mismatch promotes extra strain in the interfaces, and thus affects the bandgap. In sapphire/AlN/GdN/AlN, the differences among the thermal expansion coefficients of each material creates complex strain on GdN. GdN lattice expansion coefficient is 8.7×10^{-6}/K, while for AlN this value is 4.2×10^{-6}/K, and for sapphire substrate it is 8.1×10^{-6}/K [38-40]. As the temperature decreases to 6 K, GdN's lattice parameter shrinks more than AlN's, in such a way that the lattice mismatch between GdN and AlN causes a tensile strain on GdN's surfaces, and a compressive strain on AlN's surface, which would lead to an increase in the bandgap of GdN.

To better understand the role of thickness and temperature in a thin GdN layer, we measured the optical density (**OD**) spectra as a function of the photon energy ($\boldsymbol{E = h\nu}$), at temperatures of 300 K and 6 K, for AlN(10 nm)/GdN(*t*)/AlN(10 nm) trilayers on (0001)-sapphire with *t* = 6.3, 13, 22, 30, 80 and 350 nm (see Figs. 2 (b) and (c)). The absorption coefficient ($\boldsymbol{\alpha}$) was determined using the Beer-Lambert law that relates the amount of light absorbed by a material to its concentration, path length, and molar absorption coefficient. For a material with a uniform thickness, the relationship can be simplified as:

$$\boldsymbol{\alpha = \frac{OD}{t}}, \qquad (\mathbf{1})$$

where *t* is the film's thickness. $\boldsymbol{\alpha^2}$ versus $\boldsymbol{E}$ plots were used to estimate the direct bandgap ($\boldsymbol{E_g}$) energies of the GdN thin films via extrapolation of the linear portion of the curve to $\boldsymbol{\alpha^2 = 0}$, as shown in Fig. 2(d), where $\boldsymbol{E_g}$ = 1.6 eV. The energy at which the extrapolated line intersects the energy axis corresponds to the direct bandgap energy $\boldsymbol{E_g}$ [41-42]. To determine the indirect bandgap, the procedure is similar, but the analysis relies on extrapolating $\boldsymbol{\alpha^{1/2}}$ versus $\boldsymbol{E}$. The range of the photon energy in this investigation is well below that for the AlN bandgap of ~ 6.1 eV and sapphire bandgap of ~ 9 eV [43-45]. Thus, the observed absorption spectra are clearly attributable to the GdN films. Figures 2 (e) and (f) show $\boldsymbol{\alpha^2}$ vs. $\boldsymbol{h\nu}$ for T = 300 K, and $\boldsymbol{\alpha^{1/2}}$ vs. $\boldsymbol{h\nu}$ for T = 6 K, respectively. To reduce errors in the bandgap determination due to drawing lines manually, we identified the linear portions of each curve ($\boldsymbol{\alpha^2}$ versus $\boldsymbol{E}$) and fit the experimental data to $\boldsymbol{y = A + Bx}$. The bandgap was determined when $\boldsymbol{y = \alpha^2 = 0}$, so $\boldsymbol{E_g = -A/B}$. The uncertainty associated with this bandgap was determined using:

$$\boldsymbol{\sigma_{E_g} = \sqrt{\left(\frac{-1}{B}\cdot\sigma_A\right)^2 + \left(\frac{-A}{B^2}\cdot\sigma_B\right)^2}}, \qquad (\mathbf{2})$$

GdN Film Thickness (nm)	*A*	σ_A	*B*	σ_B	E_g	σ_{E_g}
6.3	*-7320*	*30*	*4650*	*20*	*1.576*	*0.009*
13	*-7060*	*20*	*4069*	*7*	*1.736*	*0.005*
22	*-3620*	*20*	*2117*	*7*	*1.709*	*0.009*
30	*-2258*	*2*	*1392*	*1*	*1.622*	*0.002*
80	*-388.8*	*0.8*	*261.0*	*0.4*	*1.490*	*0.004*
350	*-229.2*	*0.9*	*137.6*	*0.4*	*1.665*	*0.008*

Table I. Intercept (A) and linear fit slope (B) and their respective uncertainties (σ_A and σ_B) from $\boldsymbol{\alpha^2}$ *versus* $\boldsymbol{E}$ plots for the AlN/GdN(*t*)/AlN structures as a function of GdN thickness (*t*). The direct bandgap (*Eg*) and its uncertainty (σ_{E_g}) for GdN films at 300 K in eV units.

where σ_A and σ_B are the relevant uncertainties. Table 1 shows fitted values of the intercept (A) and slope (B) and their respective uncertainties that were used for determining the direct bandgap at 300 K. The red data points in Fig. 3 (d) show $\boldsymbol{E_g(t)}$, where the solid curve is a guide for eye and the error bars are smaller than the data points. The direct bandgap of the GdN films in the paramagnetic phase is around $\boldsymbol{E_{300K} = 1.6}$ eV and spans a region of GdN thickness (13 nm < t < 80 nm) where the gap increases as the thickness decreases, being attributed to quantum confinement. When samples are cooled down to 6 K they become FM, where the absorption spectra present more than one narrow linear deviation, indicating a spin split bandgap. Thus, in the magnetic state, the average minority (spin-down) bandgap energy is $\boldsymbol{E_\downarrow \approx 1.2}$ eV, and the average majority (spin-up) bandgap energy is $\boldsymbol{E_\uparrow \approx 0.8}$ eV, as shown by the blue data in Fig. 3 (d), where the black dotted lines correspond to their average energy values. As the temperature decreases from 300 to 6 K, the bandgap variations are $\boldsymbol{E_{300K} - E_\downarrow} \approx 0.4$ eV for the minority state and $\boldsymbol{E_{300K} - E_\uparrow \approx 0.8}$ eV for the majority state. This observed bandgap reduction as the temperature decreases to 6K suggests the shrinking of the lattice parameter in the volume of GdN overcomes the tensile strain effect at the interface of AlN/GdN that would lead to an increase in the bandgap.

Finally, Figure 3 (a) is a very simplified illustration of the band structure of a semiconducting magnetic material in its paramagnetic and ferromagnetic phases. A more accurate calculation of the GdN band structure using local density approximation can be found in [18] for the paramagnetic and ferromagnetic states. The bandgap in PM phase is the same for electrons with spin-up or spin-down, whereas in the FM phase it depends on the spin orientation, and it splits into $\boldsymbol{E_\downarrow}$ and $\boldsymbol{E_\uparrow}$. Figures 3 (b) and (c) demonstrate $\boldsymbol{\alpha^2}$ vs. $\boldsymbol{h\nu}$ plots for the direct bandgap of a 30 nm thick GdN film in both paramagnetic (300 K) and ferromagnetic (6 K) phases, respectively. In the FM

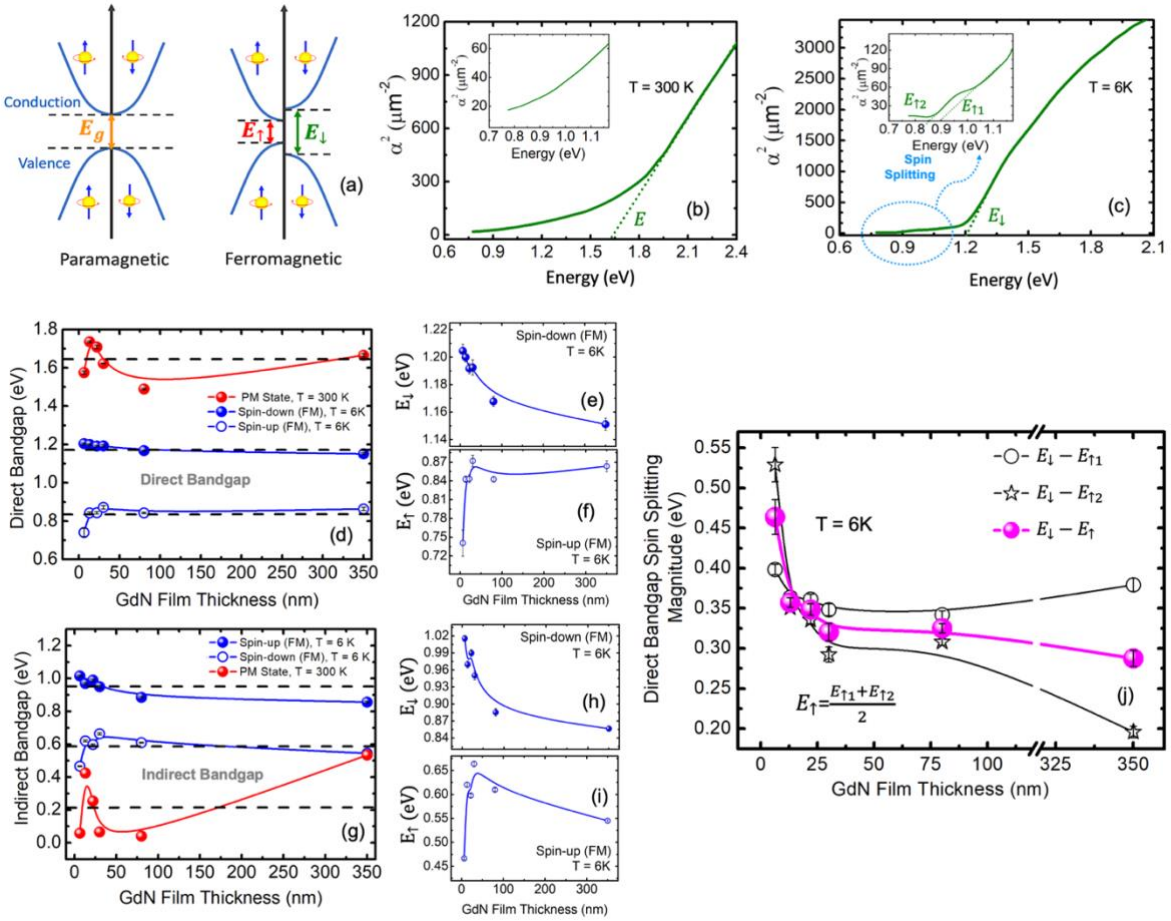


Figure 3. (a) Illustration of the band structure of a magnetic semiconductor in the paramagnetic (left) and ferromagnetic (right) phases. In the PM phase, the bandgap doesn't depend on the spin's orientation. (b) and (c) compare the $\boldsymbol{\alpha^2}$ *versus* $\boldsymbol{E}$ plots for obtaining the direct optical bandgap of sapphire/AlN(10 nm)/GdN(30 nm)/AlN(10 nm) in the PM (T = 300 K) and FM (T = 6 K) phases. In the FM phase, shown in the inset of (c), we observe more than one linear portion that is related to the spin split bandgap. (d) and (g) show the direct and indirect optical bandgaps dependence with the GdN film thickness at 300 K and 6 K, where the black dotted lines correspond to their average energy values, and (e), (f), (h) and (i) are the zoomed direct and indirect bandgaps for the minority and majority spin states at 6K. The spin splitting of the bandgap is also present in the indirect transitions. (j) Dependence of the magnitude of the spin-splitting as a function of the GdN thickness, showing that the splitting becomes larger as the film thickness decreases.

state, we observe a linear portion that extrapolates to $\boldsymbol{E_{\downarrow}} = \mathbf{1.192 \pm 0.006}$ eV, and by zooming around 0.9 eV, as shown on the inset, we observe two linear portions that extrapolate to the energies of $\boldsymbol{E_{\uparrow 2}} = \mathbf{0.844 \pm 0.005}$ eV and $\boldsymbol{E_{\uparrow 1=}}\mathbf{0.900 \pm 0.008}$, with an average value of $\boldsymbol{E_{\uparrow}} = \mathbf{0.87 \pm 0.01}$. This bandgap splitting appears for all GdN thicknesses investigated here, and a complete analysis is shown in Fig. 3 (d). The filled blue points correspond to the minority bandgap ($\boldsymbol{E_{\downarrow}}$) and the unfilled blue points correspond to the majority bandgap ($\boldsymbol{E_{\uparrow}}$). The details are shown in the zoomed Figures 3 (e) and (f), respectively. These results show a giant optical spin splitting of the direct bandgap at 6 K of $\boldsymbol{E_{\uparrow} - E_{\downarrow} \approx 0.4}$ eV. The dependence of the direct bandgap spin splitting magnitude on the GdN film thickness is shown in Fig. 3 (j). The black star and black circle points show the splitting with respect to $\boldsymbol{E_{\uparrow 1}}$ and $\boldsymbol{E_{\uparrow 2}}$, and the solid lines are guides for the eyes. As the thickness decreases, the spin-splitting magnitude increases most likely due to two combined factors: (i) The strengthening of the quantum confinement as GdN film becomes thinner; and (ii) The reduction of the GdN's volume making the surface tensile strain on GdN more relevant, thus leading to a bandgap increase.

Figure 3 (g) shows the same analysis for the indirect optical bandgaps in the PM (red points) and FM states (blue filled and unfilled points). At room temperature (300 K) the indirect transitions occur at very small energies, whereas in the FM phase, we still observe two absorption lines with separation of ~ $\mathbf{0.4}$ eV that increases as film's thickness decreases reaching values of ~ $\mathbf{0.6}$ eV for the 6.3 nm thick layer. The zoomed details are shown in Figs. 3 (h) and (f).

Our experimental results show a good agreement with the (LSDA+U) -computed band structure for $U_d = 8.0$ eV reported by Trodahl et al [18]. For a 200 nm thick GdN film capped with 200 nm of GaN, they calculated a majority-spin gap of 0.91 eV in the ferromagnetic state at 6K, and an average gap at of 1.30 eV in the paramagnetic phase at 300K, which represents a shift of 0.4 eV. The calculations also indicated an indirect-gap semiconductor with the direct gap at X and an indirect ($\boldsymbol{\Gamma}$−X) gap of 0.43 eV (0.98 eV) in the ferromagnetic (paramagnetic) state. Our data showed an average majority-spin gap around 0.84 eV at 6K, and a gap of 1.6 eV at 300K. For the indirect gap we estimated averages of 0.6 eV and 0.96 eV in the ferromagnetic phase, and 0.2 eV in the paramagnetic phase.

4. Conclusions

We investigated a set of polycrystalline GdN thin films aiming to control its bandgap and move towards their application as a spin-polarized source in spintronics devices such as spin transistors, TMR magnetic tunnel junctions and spin valves. By varying the thickness from 6 nm to 350 nm we observed a room temperature direct bandgap average value of 1.6 eV with a variation of $\mathbf{0.24}$ eV as the thickness decreases. Upon cooling the films down to 6 K, in their ferromagnetic phase the direct bandgap splits into two gaps of 1.2 eV to 0.8 eV, corresponding to the minority and majority spin bands. This giant optical spin-splitting of $\mathbf{0.4}$ eV confirms this material is suitable for spin-filtering applications. The same behavior appears in the indirect bandgap with a splitting magnitude of $\mathbf{0.3}$ eV. The observed spin splitting magnitude ($\boldsymbol{E_{\uparrow} - E_{\downarrow}}$) increased 60% as the GdN thickness decreased from 350 nm to 6 nm. This result sheds light on the manipulation and control of the optical and magnetic properties of the semiconducting GdN films with potential for high spin polarization through the spin splitting of the bandgap. Further investigations should focus on determining the bandgap dependence on a larger range of temperature covering the details on the PM-FM transition and performing X-ray measurements as a function of temperature to understand the role of thermal expansion and lattice mismatch on the bandgap.

5. Acknowledgements

This research is supported by ARO (W911NF1920041), NSF (DMR 1700137, DMR 2218550), ONR (N00014-16-1-2657, N00014-20-1-2306), the Center for Integrated Quantum Materials (NSF-DMR 1231319) and Brazilian agencies CAPES (Gilvania Vilela/POS-DOC-88881.120327/2016-01), FACEPE (APQ-0565-1.05/14), CNPq and UPE(PFA/PROGRAD/UPE 04/2017). Work at Northeastern University was partially supported by the National Science Foundation (USA) grant DMR-1905662 and the Air Force Office of Scientific Research (USA) award FA9550-20-1-0247. Work at São Paulo University was supported by FAPESP (grant 2022/15791-2).

6. References

[1] F. Natali, B. J. Ruck, N. O. V. Plank, H. J. Trodahl, S. Granville, C. Mayer, and W. R. L. Lambrecht, Rare-earth mononitrides. Prog. Mater. Sci. 58, 1316 (2013); https://doi.org/10.1016/j.pmatsci.2013.06.002

[2] C. M. Aerts, P. Strange, M. Horne, W. M. Temmerman, Z. Szotek, and A. Svane, Half-metallic to insulating behavior of rare-earth nitrides. Phys. Rev. B 69, 045115 (2004); https://doi.org/10.1103/PhysRevB.69.045115

[3] Ilia N. Sivkov, Oleg O. Brovko, and Valeri S. Stepanyuk, Spin-polarized transport properties of GdN nanocontacts. Phys. Rev. B 89, 195419 (2014); https://doi.org/10.1103/PhysRevB.89.195419

[4] Pal, A., Senapati, K., Barber, Z.H. and Blamire, M.G. (2013), Electric-Field-Dependent Spin Polarization in GdN

Spin Filter Tunnel Junctions. Adv. Mater. 25: 5581-5585 (2013); https://doi.org/10.1002/adma.201300636

[5] H. Yoshitomi, S. Kitayama, T. Kita, O. Wada, M. Fujisawa, H. Ohta, and T. Sakurai, Optical and magnetic properties in epitaxial GdN thin films. Phys. Rev. B 83, 155202 (2011); https://doi.org/10.1103/PhysRevB.83.155202

[6] Ilia N. Sivkov, Oleg O. Brovko, and Valeri S. Stepanyuk, Spin-polarized transport properties of GdN nanocontacts. Phys. Rev. B 89, 195419 (2014); https://doi.org/10.1103/PhysRevB.89.195419

[7] Chun-gang Duan, R. F. Sabiryanov, Jianjun Liu, and W. N. Mei, Strain Induced Half-Metal to Semiconductor Transition in GdN. Phys. Rev. Lett. 94, 237201 (2005); https://doi.org/10.1103/PhysRevLett.94.237201

[8] S. Granville, B. J. Ruck, A. Koo et al., Semiconducting ground state of GdN thin films. Phys. Rev. B 73, 235335 (2006); https://doi.org/10.1103/PhysRevB.73.235335

[9] P. Wachter, Physical properties of stoichiometric GdN single crystals. Results in Physics 2, 90–96 (2012); http://dx.doi.org/10.1016/j.rinp.2012.07.003

[10] Tiffany S. Santos and Jagadeesh S. Moodera, Spin Filter Tunneling. Spintronics Handbook, 2nd Edition: Spin Transport and Magnetism, CRC Press (2019). ISBN 9780429423079

[11] R. Vidyasagar, S. Kitayama, H. Yoshitomi, T. Kita1, T. Sakurai, and H. Ohta, Study on spin-splitting phenomena in the band structure of GdN. Appl. Phys. Lett. 100, 232410 (2012); https://doi.org/10.1063/1.4727903

[12] R. Vidyasagar, T. Kita, T. Sakurai, and H. Ohta, Giant optical splitting in the spin-states assisting a sharp magnetic switching in GdN thin films. Appl. Phys. Lett. 102, 222408 (2013); https://doi.org/10.1063/1.4809758

[13] Muhammad Azeem, Spin-Split Joint Density of States in GdN. Chin. Phys. Lett. 33 92), 02750 (2016); https://iopscience.iop.org/article/10.1088/0256-307X/33/2/027501

[14] D. Massarotti a, R. Caruso, A. Pal, G. Rotoli, L. Longobardi, G.P. Pepe, M.G. Blamire, F. Tafuri, Low temperature properties of spin filter NbN/GdN/NbN Josephson junctions. Physica C: Supercond. Applic. 533, pages 53-58 (2017); https://doi.org/10.1016/j.physc.2016.07.018

[15] Ahmad, H.G., Minutillo, M., Capecelatro, R. et al. Coexistence and tuning of spin-singlet and triplet transport in spin-filter Josephson junctions. Commun. Phys 5, 2 (2022). https://doi.org/10.1038/s42005-021-00783-1

[16] R. J. Gambino, T. R. McGuire, H. A. Alperin, and S. J. Pickart, Magnetic Properties and Structure of GdN and $GdN_{1-x}O_x$. J. Appl. Phys. 41, 933 (1970); https://doi.org/10.1063/1.1659030

[17] Stefan Cwik, Sebastian M. J. Beer, Stefanie Hoffmann et al. Integrating AlN with GdN Thin Films in an in Situ CVD Process: Influence on the Oxidation and Crystallinity of GdN. ACS Appl. Mater. Interfaces, 9, 27036−27044 (2017); https://doi.org/10.1021/acsami.7b08221

[18] H. J. Trodahl, A. R. H. Preston, J. Zhong, and B. J. Ruck, Ferromagnetic redshift of the optical gap in GdN. Phys. Rev. B 76, 085211 (2007); https://doi.org/10.1103/PhysRevB.76.085211

[19] R. Vidyasagar, T. Kita, T. Sakurai, and H. Ohta, Electronic transitions in GdN band structure. J. Appl. Phys. 115, 203717 (2014); https://doi.org/10.1063/1.4880398

[20] F. Leuenberger, A. Parge,W. Felsch, K. Fauth, and M. Hessler, GdN thin films: Bulk and local electronic and magnetic properties. Phys. Rev. B 72, 014425 (2005); https://doi.org/10.1103/PhysRevB.72.014427

[21] J. Tauc, Optical Properties and Electronic Structure of Amorphous Ge and Si. Mat. Res. Bull. Vol. 3, pp. 37-46(1968). Pergamon Press, Inc. Printed in the United States.

[22] A. R. Zanatta, Revisiting the optical bandgap of semiconductors and the proposal of a unified methodology to its determination. Scientific Reports 9, 11225, (2019); https://doi.org/10.1038/s41598-019-47670-y

[23] Ali Shaib et al., Coexisting structural phases in the catalytically driven growth of rock salt GdN. Materials Research Express 7, 046404 (2020); https://doi.org/10.1088/2053-1591/ab802f

[24] Kartik Senapati, Thomas Fix, Mary E. Vickers, Mark G. Blamire, and Zoe H. Barber, Structural evolution and competing magnetic orders in polycrystalline GdN films. Physical Review B 83, 014403 (2011); https://doi.org/10.1103/PhysRevB.83.014403

[25] P. Wachter, E. Kaldis, Magnetic interaction in GdN and GdN1−xOx. Journal of Magnetism and Magnetic Materials,Volumes 15–18, Part 1, pages 305-306, (1980); https://doi.org/10.1016/0304-8853(80)91062-8

[26] K. Khazen, H. J. von Bardeleben, J. L. Cantin, A. Bittar, S. Granville, H. J. Trodahl, and B. J. Ruck, Ferromagnetic resonance study of GdN thin films with bulk and extended lattice constants. Physical Review B 74, 245330, (2006); https://doi.org/10.1103/PhysRevB.74.245330

[27] Li, D. X., Haga, Y., Shida, H., Suzuki, T., Kwon, Y. S., & Kido, G. (1997). Magnetic properties of stoichiometric Gd monopnictides. Journal of Physics Condensed Matter, 9(48), 10777-10788. https://doi.org/10.1088/0953-8984/9/48/019

[28] M.A. Scarpulla et al., Molecular beam epitaxy of ferromagnetic epitaxial GdN thin films. Journal of Crystal Growth 404, 146–151(2014); http://dx.doi.org/10.1016/j.jcrysgro.2014.07.010

[29] J. R. Chan et al. Temperature-Induced Four-Fold-on-Six-Fold Symmetric Heteroepitaxy, Rocksalt SmN on Hexagonal AlN.Cryst. Growth Des., 16, 11, 6454–6460 (2016); https://doi.org/10.1021/acs.cgd.6b01133

[30] Y. P. Varshni, Temperature dependence of the energy gap in semiconductors, Physica 34, 149 (1967); https://doi.org/10.1016/0031-8914(67)90062-6

[31] P.B. Allen and M. Cardona, Temperature dependence of the direct gap of Si and Ge, Phys. Rev. B 27, 4760 (1983); https://doi.org/10.1103/PhysRevB.27.4760

[32] Gaponenko, S. and Demir, H., Quantum confinement effects in semiconductors, Applied Nanophotonics (pp. 52-91). Cambridge: Cambridge University Press. https://doi.org/10.1017/9781316535868.004

[33] P. Dey, J. Paul, J. Bylsma, D. Karaiskaj, J.M. Luther, M.C. Beard, A.H. Romero, Origin of the temperature dependence of the band gap of PbS and PbSe quantum dots, Sol. State Comm. 165, 49 (2013); http://dx.doi.org/10.1016/j.ssc.2013.04.022

[34] M. Li and J.C. Li, Size effects on the band-gap of semiconductor compounds, Materials Letters 60, 2526–2529, (2006); https://doi.org/10.1016/j.matlet.2006.01.032

[35] M Singha, BM Taele, M Goyal, Modeling of size and shape dependent band gap, dielectric constant and phonon frequency of semiconductor nanosolids, Chinese J. Phys. 70, 26–36 (2021); https://doi.org/10.1016/j.cjph.2021.01.001

[36] A. Barnasas et al., Quantum confinement effects of thin ZnO films by experiment and theory, Physica E 120, 114072 (2020); https://doi.org/10.1016/j.physe.2020.114072

[37] B Bertheville, H Bill and H Hagemann, Experimental Raman scattering investigation of phonon anharmonicity effects in Li_2S, J. Phys.: Condens. Matter 10, 2155 (1998); https://dx.doi.org/10.1088/0953-8984/10/9/018

[38] D. A. Shohonov et al., Effects of lattice parameter manipulations on electronic and optical properties of BaSi2, Thin Sol. Films 686, 137436 (2019); https://doi.org/10.1016/j.tsf.2019.137436

[39] Gyeonghun Kim and Sangjoon Ahn, Thermal conductivity of gadolinium added uranium mononitride fuel pellets sintered by spark plasma sintering, J. Nuc. Mater. 546, 15278 (2021); https://doi.org/10.1016/j.jnucmat.2021.152785

[40] W. M. Yim and R. J. Paff, Thermal expansion of AlN, sapphire, and silicon, J. Appl. Phys. 45, 1456 (1974); https://doi.org/10.1063/1.1663432

[41] P. Y. Yu and M. Cardona, Fundamentals of Semiconductors, Physics and Materials Properties. Springer, 4th Edition, (2010);http://doi.org/10.1007/978-3-642-00710-1

[42] J. I. Pankove and D. A. Kiewit, Optical Processes in Semiconductors. J. Electrochem. Soc. 119 156Ca (1972); http://doi.org/10.1149/1.2404256

[43] Xiao Tang, Fazla Hossain, Kobchat Wongchotigul, and Michael G. Spencer, Near band-edge transition in aluminum nitride thin films grown by metal organic chemical vapor deposition. Appl. Phys. Lett. 72, 1501 (1998); https://doi.org/10.1063/1.121039

[44] J. A. Pérez Taborda, H. Riascos Landázuri and L. P. V. Londoño, Correlation Between Optical, Morphological, and Compositional Properties of Aluminum Nitride Thin Films by Pulsed Laser Deposition. IEEE Sensors Journal 16, (2), 359-364 (2016), https://doi.org/10.1109/JSEN.2015.2466467

[45] Alang Kasim Harman, Susumu Ninomiya, and Sadao Adachi, Optical constants of sapphire (α-Al2O3) single crystals. J.Appl. Phys. 76, 8032 (1994); https://doi.org/10.1063/1.357922